

Diverse soliton solutions and dynamical analysis of the discrete coupled mKdV equation with 4×4 Lax pair

Xue-Ke Liu(刘雪珂) and Xiao-Yong Wen(闻小永)
Citation: Chin. Phys. B, 2023, 32 (**12**): 120203. DOI: 10.1088/1674-1056/acf122
Journal homepage: http://cpb.iphy.ac.cn; http://iopscience.iop.org/cpb

What follows is a list of articles you may be interested in

Interaction solutions and localized waves to the (2+1)-dimensional Hirota-Satsuma-Ito equation with variable coefficient

Xinying Yan(闫鑫颖), Jinzhou Liu(刘锦洲), and Xiangpeng Xin(辛祥鹏)
Chin. Phys. B, 2023, 32 (**7**): 070201. DOI: 10.1088/1674-1056/acb9f2

Resonant interactions among two-dimensional nonlinear localized waves and lump molecules for the (2+1)-dimensional elliptic Toda equation

Fuzhong Pang(庞福忠), Hasi Gegen(葛根哈斯), and Xuemei Zhao(赵雪梅)
Chin. Phys. B, 2023, 32 (**5**): 050205. DOI: 10.1088/1674-1056/acb2c2

Soliton interactions and asymptotic state analysis in a discrete nonlocal nonlinear self-dual network equation of reverse-space type

Cui-Lian Yuan(袁翠连) and Xiao-Yong Wen(闻小永)
Chin. Phys. B, 2021, 30 (**3**): 030201. DOI: 10.1088/1674-1056/abc2ba

Multi-soliton solutions for the coupled modified nonlinear Schrödinger equations via Riemann-Hilbert approach

Zhou-Zheng Kang(康周正), Tie-Cheng Xia(夏铁成), Xi Ma(马茜)
Chin. Phys. B, 2018, 27 (**7**): 070201. DOI: 10.1088/1674-1056/27/7/070201

Painlevé integrability of generalized fifth-order KdV equation with variable coefficients: Exact solutions and their interactions

Xu Gui-Qiong (徐桂琼)
Chin. Phys. B, 2013, 22 (**5**): 050203. DOI: 10.1088/1674-1056/22/5/050203

Diverse soliton solutions and dynamical analysis of the discrete coupled mKdV equation with 4×4 Lax pair

Xue-Ke Liu(刘雪珂) and Xiao-Yong Wen(闻小永)[†]

School of Applied Science, Beijing Information Science and Technology University, Beijing 100192, *China*

(Received 22 July 2023; revised manuscript received 8 August 2023; accepted manuscript online 17 August 2023)

Under consideration in this study is the discrete coupled modified Korteweg–de Vries (mKdV) equation with 4×4 Lax pair. Firstly, through using continuous limit technique, this discrete equation can be mapped to the coupled KdV and mKdV equations, which may depict the development of shallow water waves, the optical soliton propagation in cubic nonlinear media and the Alfven wave in a cold collision-free plasma. Secondly, the discrete generalized $(r,N-r)$-fold Darboux transformation is constructed and extended to solve this discrete coupled equation with the fourth-order linear spectral problem, from which diverse exact solutions including usual multi-soliton and semi-rational soliton solutions on the vanishing background, higher-order rational soliton and mixed hyperbolic-rational soliton solutions on the non-vanishing background are derived, and the limit states of some soliton and rational soliton solutions are analyzed by the asymptotic analysis technique. Finally, the numerical simulations are used to explore the dynamical behaviors of some exact soliton solutions. These results may be helpful for understanding some physical phenomena in fields of shallow water wave, optics, and plasma physics.

Keywords: discrete coupled mKdV equation, continuous limit, discrete generalized $(r,N-r)$-fold Darboux transformation, multi-soliton solutions, rational soliton solutions

PACS: 02.30.Ik, 05.45.Yv, 04.60.Nc **DOI:** 10.1088/1674-1056/acf122

1. Introduction

Solitons are a class of nonlinear localized waves with particle-like properties,[1] which have been brought to light in various physical areas, including nonlinear optics, plasma physics, electricity, quantum mechanics, opening up new applications in these fields.[2–5] The history of soliton can be traced back to 1834, the year in which John Scott Russell unexpectedly discovered the phenomenon of solitary wave in a canal. However, it was only with the proposal of the Korteweg–de Vries (KdV) equation from which soliton theory gained massive attention. The most notable feature of solitons is that they can keep the shapes and velocities unaltered while the solitary waves propagate forward.[2] Nonlinear partial differential equations (NPDEs) may model various physical phenomena in optics, biology, plasma, and other research fields.[6–8] However, for some events such as the motion of one-dimensional particles, the propagation of pulses in biological chains and transmission of electrical signals in nonlinear inductance-capacitance circuits,[1,8–11] the discrete nonlinear equations serve as more appropriate descriptions compared with NPDEs. The main motivation for studying the discrete nonlinear equation is that they can keep some characteristics of the original continuous equations unaltered.[12] In Ref. [13], the authors put forward and studied the initial value problem of the following N-component discrete modified Korteweg–de Vries (mKdV) equation

$$\frac{\partial u_n^{(i)}}{\partial t}=\Big(1+\sum_{j,k=1}^{N}C_{jk}u_n^{(j)}u_n^{(k)}\Big)\Big(u_{n+1}^{(i)}-u_{n-1}^{(i)}\Big),\quad i=1,\,2,\ldots,\,N,\tag{1}$$

where $u_n^{(i)}=u^{(i)}(n,t)$ are functions relying on the discrete spatial variable n and continuous temporal variable t, C_{jk} are arbitrary constants. In Ref. [14], Eq. (1) has converged to the N-component continuous mKdV equation under the continuous limit. When $N=2$ and $C_{12}=C_{21}=0$, Eq. (1) degenerates into the following discrete coupled mKdV equation:[15]

$$\begin{cases}X_{n,t}=(1+X_n^2+Y_n^2)(X_{n+1}-X_{n-1}),\\ Y_{n,t}=(1+X_n^2+Y_n^2)(Y_{n+1}-Y_{n-1}),\end{cases}\tag{2}$$

where $X_n=X(n,t)$, $X_{n,t}=\frac{\mathrm{d}X_n}{\mathrm{d}t}$, $Y_n=Y(n,t)$, $Y_{n,t}=\frac{\mathrm{d}Y_n}{\mathrm{d}t}$, whose Lax pair has the following matrix form:[15]

$$\begin{aligned}\Psi_{n+1}&=A_n\Psi_n=\begin{pmatrix}\lambda I & A_{1,n}\\ -A_{1,n} & \frac{I}{\lambda}\end{pmatrix}\Psi_n,\\ \Psi_{n,t}&=B_n\Psi_n=\begin{pmatrix}\lambda^2I+B_{1,n} & B_{2,n}\\ B_{3,n} & \frac{I}{\lambda}+B_{1,n}\end{pmatrix}\Psi_n.\end{aligned}\tag{3}$$

Here, λ is the spectral parameter, I is a 2×2 unit matrix and

$$A_{1,n}=\begin{pmatrix}X_n & Y_n\\ Y_n & -X_n\end{pmatrix},$$
$$B_{1,n}=\begin{pmatrix}X_nX_{n-1}+Y_nY_{n-1} & X_nY_{n-1}-X_{n-1}Y_n\\ -X_nY_{n-1}+X_{n-1}Y_n & X_nX_{n-1}+Y_nY_{n-1}\end{pmatrix},$$

[†]Corresponding author. E-mail: xiaoyongwen@163.com

© 2023 Chinese Physical Society and IOP Publishing Ltd

$$B_{2,n}=\begin{pmatrix} X_n\lambda+\frac{X_{n-1}}{\lambda} & Y_n\lambda+\frac{Y_{n-1}}{\lambda} \\ Y_n\lambda+\frac{Y_{n-1}}{\lambda} & -X_n\lambda-\frac{X_{n-1}}{\lambda} \end{pmatrix},$$
$$B_{3,n}=\begin{pmatrix} -X_{n-1}\lambda-\frac{X_n}{\lambda} & -Y_{n-1}\lambda-\frac{Y_n}{\lambda} \\ -Y_{n-1}\lambda-\frac{Y_n}{\lambda} & X_{n-1}\lambda+\frac{X_n}{\lambda} \end{pmatrix}.$$

Equation (3) can yield Eq. (2) by zero-curvature equation $A_{n,t}+A_nB_n-B_{n+1}A_n=0$. When $Y_n=0$, Eq. (2) reduces to the single component discrete mKdV equation, whose solitonic interactions and conservation laws of the discrete mKdV equation have been studied in Ref. [16]. This equation is also known as the so-called Volterra equation, which may be in connection with the spectrum of Langmuir wave in plasma physics.[1] In Ref. [15], the generalized symmetry and polynomial conserved densities of Eq. (2) have been obtained. Equation (2) can also be turned into the continuous coupled mKdV equation[15]

$$\begin{cases} X_\tau+6(X^2+Y^2)X_x+X_{xxx}=0, \\ Y_\tau+6(X^2+Y^2)Y_x+Y_{xxx}=0, \end{cases} \tag{4}$$

through the limit conditions

$$X_n=\delta X\left[(n+2t)\delta,\frac{1}{3}\delta^3 t\right]+O(\delta^2)\equiv\delta X(x,\tau)+O(\delta^2),$$
$$Y_n=\delta Y\left[(n+2t)\delta,\frac{1}{3}\delta^3 t\right]+O(\delta^2)\equiv\delta Y(x,\tau)+O(\delta^2),$$

where $\delta\ll 1$, X and Y are functions of the continuous spatial variable x and temporal variable τ, $X_\tau=\frac{\partial X}{\partial\tau}$, $X_x=\frac{\partial X}{\partial x}$, $X_{xxx}=\frac{\partial^3 X}{\partial x^3}$, $Y_\tau=\frac{\partial Y}{\partial\tau}$, $Y_x=\frac{\partial Y}{\partial x}$, $Y_{xxx}=\frac{\partial^3 Y}{\partial x^3}$. When $Y=0$, Eq. (4) is turned into the well-known mKdV equation, which has been extensively used to depict the optical soliton propagation in cubic nonlinear media involving ultrashort pulses[17,18] and the Alfven wave in a cold collision-free plasma.[19] Correspondingly, its discrete forms may also well describe certain physical phenomena.

Some methods for obtaining the exact solutions of discrete integrable equations include the inverse scattering method,[20,21] Riemann–Hilbert method,[22,23] algebraic geometry method,[24] Darboux transformation (DT),[16,25,26] and so on. Among them, the DT is one of the available methods, whose basic idea is to keep the Lax pair of discrete equations covariant. Recently, the discrete generalized $(r,N-r)$-fold DT technique has been proposed and successfully applied to solve some continuous equations, $(2+1)$-dimensional equations and discrete equations.[27–29] Generally speaking, the discrete N-fold DT can only obtain solitons, while the discrete generalized $(r,N-r)$-fold DT can obtain more types of exact solutions, including soliton solutions, rational, semi-rational and their mixed interaction solutions. At present, while the discrete generalized $(r,N-r)$-fold DT has been primarily utilized for addressing the discrete integrable equations related to 2×2 Lax pair,[11,16,30–32] the research on discrete equations pertaining to 4×4 Lax pair is still rare.[33,34] Therefore, it is significant to extend this method from 2×2 Lax pair to 4×4 Lax pair. To our knowledge, the generalized symmetry and polynomial conserved densities of Eq. (2) have been obtained, whereas there is no relevant research on the higher-order exact solutions like multi-soliton, higher-order semi-rational soliton (SRS), higher-order rational soliton (RS) and mixed interaction soliton solution of Eq. (2). Therefore, in this study, our main interest is to consider multi-soliton and higher-order SRS solutions on the vanishing background, higher-order RS and mixed interaction soliton solutions on the non-vanishing background of Eq. (2) through the discrete generalized $(r,N-r)$-fold DT. Meanwhile, we perform numerical simulation and asymptotic analysis to analyze the dynamical properties and limit states of some exact solutions.

The rest contents of this paper contain three sections. In Section 2, the continuous limit is used to map Eq. (2) to the coupled KdV equation and a new nonlinear equation without dispersion term. In Section 3, we construct the discrete generalized $(r,N-r)$-fold DT for Eq. (2), from which the usual multi-soliton, SRS, RS and mixed interaction soliton solutions are given. Moreover, the asymptotic states and numerical simulations of some soliton and rational solutions are also discussed. In Section 4, we give our conclusions.

2. Continuous limit

Continuous limit is a powerful tool to connect the discrete and continuous equations. Due to the fact that the discrete single component mKdV equation can converge to the continuous KdV and mKdV equations under the continuous limit,[35] the discrete coupled mKdV equation (2) may also converge to the continuous coupled KdV and mKdV equations. In Ref. [15], Eq. (2) has been mapped to the coupled mKdV equation (4). In what follows, we will construct the new continuous conditions that make Eq. (2) correspond to two continuous equations.

(i) Equation (2) corresponds to the continuous coupled KdV equation[36,37]

$$\begin{cases} X_\tau-4(X+Y)X_x-X_{xxx}=0, \\ Y_\tau-4(X+Y)Y_x-Y_{xxx}=0, \end{cases} \tag{5}$$

through the continuous conditions

$$X_n=1+\delta^2X[(n+6t)\delta,\delta^3t]\equiv 1+\delta^2X(x,\tau)+O(\delta^3),$$
$$Y_n=1+\delta^2Y[(n+6t)\delta,\delta^3t]\equiv 1+\delta^2Y(x,\tau)+O(\delta^3).$$

It should be noted that the coefficients of Eq. (5) are different from the coefficients of the coupled KdV equation in Refs. [36,37]. In Ref. [36], when selecting special coefficients, Eq. (5) can be derived from a two-layer fluid system. In Ref. [37], the Lax pair of the coupled KdV equation with different coefficients has been constructed via the prolongation structure technique. When $Y=0$, Eq. (5) is transformed into the KdV equation, which has been shown to describe the

asymptotic development of shallow water waves[38] and ion-acoustic waves.[39]

(ii) When taking the limit conditions

$$X_n = 1 + X(\delta n, \delta t) \equiv 1 + X(x,\tau),$$
$$Y_n = 1 + Y(\delta n, \delta t) \equiv 1 + Y(x,\tau),$$

a set of new nonlinear equations

$$\begin{cases} X_\tau - 2(X^2+Y^2+2X+2Y+3)X_x = 0, \\ Y_\tau - 2(X^2+Y^2+2X+2Y+3)Y_x = 0, \end{cases} \tag{6}$$

can be obtained. Certainly, Eq. (6) can also reduce to a new single component equation without dispersion term if $Y = 0$.

Therefore, we can conclude that a discrete equation can correspond to different NPDEs under different continuous limits. Equation (6) is a new NPDE without dispersion term, which is worth further research.

3. Discrete generalized $(r, N-r)$-fold DT

In this section, we will build the discrete generalized $(r,N-r)$-fold DT for Eq. (2). To begin with, we presume that $\Psi_n(\lambda_i) = (\Psi_{1,n}(\lambda_i),\ \Psi_{2,n}(\lambda_i),\ \Psi_{3,n}(\lambda_i),\ \Psi_{4,n}(\lambda_i))^{\mathrm{T}}$ $(i = 1,\ 2,\ 3,\ldots,\ r)$ are r different fundamental solutions of Eq. (3) based on the initial seed solutions X_n and Y_n. Then we consider the following gauge transformation:

$$\widetilde{\Psi}_n = G_n \Psi_n = \begin{pmatrix} O_n & R_n & S_n & T_n \\ -R_n & O_n & T_n & -S_n \\ U_n & V_n & C_n & D_n \\ V_n & -U_n & -D_n & C_n \end{pmatrix} \Psi_n, \tag{7}$$

with

$$O_n = \lambda^{2N} + \sum_{j=0}^{N-1} a_n^{(2j)} \lambda^{2j},\ \ R_n = \sum_{j=0}^{N-1} b_n^{(2j)} \lambda^{2j},$$
$$S_n = -\sum_{j=1}^{N} c_n^{(2N-2j+1)} \lambda^{2j-1},$$
$$T_n = -\sum_{j=1}^{N} d_n^{(2N-2j+1)} \lambda^{2j-1},$$
$$U_n = \sum_{j=1}^{N} c_n^{(2j-1)} \lambda^{2j-1},\ \ V_n = \sum_{j=1}^{N} d_n^{(2j-1)} \lambda^{2j-1},$$
$$C_n = \sum_{j=1}^{N} a_n^{(2N-2j)} \lambda^{2j} + 1,\ \ D_n = \sum_{j=1}^{N} b_n^{(2N-2j)} \lambda^{2j},$$

where $a_n^{(2j)}$, $b_n^{(2j)}$, $c_n^{(2N-2j+1)}$ and $d_n^{(2N-2j+1)}$ are determined by the following $4N$ equations $(N = r + \sum_{i=1}^{r} p_i)$:

$$G_n^{(0)}(\lambda_i)\Psi_n^{(0)}(\lambda_i) = 0,$$
$$G_n^{(0)}(\lambda_i)\Psi_n^{(1)}(\lambda_i) + G_n^{(1)}(\lambda_i)\Psi_n^{(0)}(\lambda_i) = 0,$$
$$G_n^{(0)}(\lambda_i)\Psi_n^{(2)}(\lambda_i) + G_n^{(1)}(\lambda_i)\Psi_n^{(1)}(\lambda_i) + G_n^{(2)}(\lambda_i)\Psi_n^{(0)}(\lambda_i) = 0,$$
$$\cdots,$$
$$\Sigma_{j=0}^{p_i} G_n^{(j)}(\lambda_i)\Psi_n^{(p_i-j)}(\lambda_i) = 0,$$

where $G_n^{(i)}$ is expressed by binomial expansion $G_n(\lambda_i + \varepsilon) = G_n^{(0)} + G_n^{(1)}\varepsilon + \cdots + G_n^{(2N)}\varepsilon^{2N}$ and $\Psi_n^{(k)}$ is obtained by the Taylor expansion $\Psi_n(\lambda_i+\varepsilon) = \Psi_n^{(0)}(\lambda_i) + \Psi_n^{(1)}(\lambda_i)\varepsilon + \Psi_n^{(2)}(\lambda_i)\varepsilon^2 + \cdots$, in which $\Psi_n^{(k)}(\lambda_i) = \frac{1}{k!}\frac{\partial^k}{\partial \lambda_i^k}\Psi(\lambda_i)$. Based on the transformation (7), Ψ_n is transformed into $\widetilde{\Psi}_n$, whose Lax pair has the following forms: $\widetilde{\Psi}_{n+1} = \widetilde{A}_n\widetilde{\Psi}_n$ and $\widetilde{\Psi}_{n,t} = \widetilde{B}_n\widetilde{\Psi}_n$, in which $\widetilde{A}_n$ and $\widetilde{B}_n$ meet two transformation relations $\widetilde{A}_n = G_{n+1}A_nG_n^{-1}$ and $\widetilde{B}_n = (G_{n,t} + G_nB_n)G_n^{-1}$ having the same forms as A_n and B_n, respectively, where the superscript -1 stands for the inverse matrix.

The above process can be summarized as the following discrete generalized $(r,N-r)$-fold DT theorem.

Theorem 1 Let

$$\Psi_n(\lambda_i) = (\Psi_{1,n}(\lambda_i), \Psi_{2,n}(\lambda_i), \Psi_{3,n}(\lambda_i), \Psi_{4,n}(\lambda_i))^{\mathrm{T}}$$

be r different column vector solutions with spectral parameters λ_i $(i = 1,2,\ldots,r)$ and the seed solutions X_n, Y_n of Eq. (2), then the relations between the old solutions X_n, Y_n and new solutions $\widetilde{X}_n$, $\widetilde{Y}_n$ are given as follows:

$$\widetilde{X}_n = a_{n+1}^{(0)}X_n + b_{n+1}^{(0)}Y_n - c_{n+1}^{(2N-1)},$$
$$\widetilde{Y}_n = a_{n+1}^{(0)}Y_n - b_{n+1}^{(0)}X_n - d_{n+1}^{(2N-1)}, \tag{8}$$

where $a_{n+1}^{(0)}$, $b_{n+1}^{(0)}$, $c_{n+1}^{(2N-1)}$ and $d_{n+1}^{(2N-1)}$ can be given by replacing n in $a_n^{(0)}$, $b_n^{(0)}$, $c_n^{(2N-1)}$ and $d_n^{(2N-1)}$ with $n+1$, in which

$$a_n^{(0)} = \frac{\Delta a_n^{(0)}}{\Delta_N^{\varepsilon(r)}},\ b_n^{(0)} = \frac{\Delta b_n^{(0)}}{\Delta_N^{\varepsilon(r)}},\ c_n^{(2N-1)} = \frac{\Delta c_n^{(2N-1)}}{\Delta_N^{\varepsilon(r)}},$$
$$d_n^{(2N-1)} = \frac{\Delta d_n^{(2N-1)}}{\Delta_N^{\varepsilon(r)}},\ \Delta_N^{\varepsilon(r)} = \det\begin{pmatrix} \Delta^{(1)} \\ \Delta^{(2)} \\ \cdots \\ \Delta^{(r)} \end{pmatrix}, \tag{9}$$

where $\Delta^{(i)} = (\Delta_{j,s}^{(i)})_{4(p_i+1)\times 4N}$, in which $\Delta_{j,s}^{(r)}$ $(1 \le j \le 4(p_i+1),\ \ 1 \le s \le 4N,\ \ i = 1,2,\ldots,r)$ are given by the following formulae:

$$\Delta_{j,s}^{(i)} = \Sigma_{k=0}^{j-1} C_{2N-2s}^{k} \lambda_i^{2N-2s-k} \Psi_{1,n}^{(j-1-k)},$$
$$\text{for } 1 \le j \le p_i+1,\ \ 1 \le s \le N,$$
$$\Delta_{j,s}^{(i)} = \Sigma_{k=0}^{j-1} C_{4N-2s}^{k} \lambda_i^{4N-2s-k} \Psi_{2,n}^{(j-1-k)},$$
$$\text{for } 1 \le j \le p_i+1,\ \ N+1 \le s \le 2N,$$
$$\Delta_{j,s}^{(i)} = -\Sigma_{k=0}^{j-1} C_{2s-4N-1}^{k} \lambda_i^{2s-4N-1-k} \Psi_{3,n}^{(j-1-k)},$$
$$\text{for } 1 \le j \le p_i+1,\ \ 2N+1 \le s \le 3N,$$
$$\Delta_{j,s}^{(i)} = -\Sigma_{k=0}^{j-1} C_{2s-6N-1}^{k} \lambda_i^{2s-6N-1-k} \Psi_{4,n}^{(j-1-k)},$$
$$\text{for } 1 \le j \le p_i+1,\ \ 3N+1 \le s \le 4N,$$
$$\Delta_{j,s}^{(i)} = \Sigma_{k=0}^{j-N-1} C_{2N-2s}^{k} \lambda_i^{2N-2s-k} \Psi_{2,n}^{(j-N-1-k)},$$
$$\text{for } p_i+2 \le j \le 2(p_i+1),\ \ 1 \le s \le N,$$
$$\Delta_{j,s}^{(i)} = -\Sigma_{k=0}^{j-N-1} C_{4N-2s}^{k} \lambda_i^{4N-2s-k} \Psi_{1,n}^{(j-N-1-k)},$$

$$
\begin{aligned}
&\text{for } p_i+2\le j\le 2(p_i+1),\ N+1\le s\le 2N,\\
\Delta_{j,s}^{(i)}=&\Sigma_{k=0}^{j-N-1}C_{2s-4N-1}^{k}\lambda_i^{2s-4N-1-k}\Psi_{4,n}^{(j-N-1-k)},\\
&\text{for } p_i+2\le j\le 2(p_i+1),\ 2N+1\le s\le 3N,\\
\Delta_{j,s}^{(i)}=&-\Sigma_{k=0}^{j-N-1}C_{2s-6N-1}^{k}\lambda_i^{2s-6N-1-k}\Psi_{3,n}^{(j-N-1-k)},\\
&\text{for } p_i+2\le j\le 2(p_i+1),\ 3N+1\le s\le 4N,\\
\Delta_{j,s}^{(i)}=&\Sigma_{k=0}^{j-2N-1}C_{2s}^{k}\lambda_i^{2l-k}\Psi_{3,n}^{(h-2N-1-k)},\\
&\text{for } 2p_i+3\le j\le 3(p_i+1),\ 1\le s\le N,\\
\Delta_{j,s}^{(i)}=&\Sigma_{k=0}^{j-2N-1}C_{2s-2N}^{k}\lambda_i^{2s-2N-k}\Psi_{4,n}^{(h-2N-1-k)},\\
&\text{for } 2p_i+3\le j\le 3(p_i+1),\ N+1\le s\le 2N,\\
\Delta_{j,s}^{(i)}=&\Sigma_{k=0}^{j-2N-1}C_{6N-2s+1}^{k}\lambda_i^{6N-2s+1-k}\Psi_{1,n}^{(h-2N-1-k)},\\
&\text{for } 2p_i+3\le j\le 3(p_i+1),\ 2N+1\le s\le 3N,\\
\Delta_{j,s}^{(i)}=&\Sigma_{k=0}^{j-2N-1}C_{8N-2s+1}^{k}\lambda_i^{8N-2s+1-k}\Psi_{2,n}^{(h-2N-1-k)},\\
&\text{for } 2p_i+3\le j\le 3(p_i+1),\ 3N+1\le s\le 4N,\\
\Delta_{j,s}^{(i)}=&\Sigma_{k=0}^{j-3N-1}C_{2s}^{k}\lambda_i^{2s-k}\Psi_{4,n}^{(j-3N-1-k)},\\
&\text{for } 3p_i+4\le j\le 4(p_i+1),\ 1\le s\le N,\\
\Delta_{j,s}^{(i)}=&-\Sigma_{k=0}^{j-3N-1}C_{2s-2N}^{k}\lambda_i^{2s-2N-k}\Psi_{3,n}^{(j-3N-1-k)},\\
&\text{for } 3p_i+4\le j\le 4(p_i+1),\ N+1\le s\le 2N,\\
\Delta_{j,s}^{(i)}=&-\Sigma_{k=0}^{j-3N-1}C_{6N-2s+1}^{k}\lambda_i^{6N-2s+1-k}\Psi_{2,n}^{(j-3N-1-k)},\\
&\text{for } 3p_i+4\le j\le 4(p_i+1),\ 2N+1\le s\le 3N,\\
\Delta_{j,s}^{(i)}=&\Sigma_{k=0}^{j-3N-1}C_{8N-2s+1}^{k}\lambda_i^{8N-2s+1-k}\Psi_{1,n}^{(j-3N-1-k)},\\
&\text{for } 3p_i+4\le j\le 4(p_i+1),\ 3N+1\le s\le 4N,
\end{aligned}
$$

and $\Delta a_n^{(0)}$, $\Delta b_n^{(0)}$, $\Delta c_n^{(2N-1)}$ and $\Delta d_n^{(2N-1)}$ are obtained by replacing the Nth, $2N$th, $(2N+1)$th and $(3N+1)$th of $\Delta_N^{\varepsilon(r)}$ by the column vector $(z^{(1)},\ z^{(2)},\ldots,\ z^{(r)})^{\mathrm{T}}$ with $z^{(i)}=(z_j^i)_{4(p_i+1)\times 1}$ in which

$$
\begin{aligned}
z_j^i=&-\Sigma_{k=0}^{j-1}C_{2N}^{k}\lambda_i^{2N-k}\Psi_{1,n}^{(j-1-k)},\\
&\text{for}\quad 1\le j\le p_i+1,\\
z_j^i=&-\Sigma_{k=0}^{j-N-1}C_{2N}^{k}\lambda_i^{2N-k}\Psi_{2,n}^{(j-N-1-k)},\\
&\text{for}\quad p_i+2\le j\le 2(p_i+1),\\
z_j^i=&-\Psi_{3,z}^{(j-2N-1)},\ \text{for}\ 2p_i+3\le j\le 3(p_i+1),\\
z_j^i=&-\Psi_{4,z}^{(j-3N-1)},\ \text{for}\ 3p_i+4\le j\le 4(p_i+1).
\end{aligned}
$$

Remark 1 In the above theorem, r is the number of spectral parameter λ_i, N is the order number of DT and $N-r$ is the sum of the order number of the highest derivative of the Darboux matrix G_n or the vector eigenfunction Ψ_n. The N-fold DT can be derived from Theorem 1 by selecting N spectral parameters and without expanding Ψ_n into Taylor series, from which we can obtain the soliton solutions on zero background. When $r=1$, Theorem 1 reduces to the $(1,N-1)$-fold DT, which can yield higher-order rational and semi-rational solutions on nonzero background. When $1<r<N$, diverse mixed interaction solutions can be derived through Theorem 1. In the next several subsections, we will use Theorem 1 to give multi-soliton solution, rational solutions and their mixed interaction solutions.

3.1. Multi-soliton and higher-order SRS solutions on the vanishing background

Based on the zero seed solutions $X_n=Y_n=0$, the fundamental solution of Eq. (2) can be given by

$$
\Psi_n=\begin{pmatrix}
C_1\lambda^n\mathrm{e}^{\lambda^2 t+\theta(\varepsilon)}\\
C_2\lambda^n\mathrm{e}^{\lambda^2 t+\theta(\varepsilon)}\\
C_3\frac{1}{\lambda^n}\mathrm{e}^{\frac{t}{\lambda^2}-\theta(\varepsilon)}\\
C_4\frac{1}{\lambda^n}\mathrm{e}^{\frac{t}{\lambda^2}-\theta(\varepsilon)}
\end{pmatrix},\tag{10}
$$

where C_i $(i=1,\ 2,\ 3,\ 4)$ are arbitrary constants. We need to declare that $\theta(\varepsilon)=0$ when seeking the soliton solutions and $\theta(\varepsilon)=2\Sigma_{k=0}^{N-1}e_k\varepsilon^k$ when seeking the SRS solutions.

3.1.1. Multi-soliton solutions

When $N=r=1$ and Taylor expansion is not performed on spectral parameter λ_1, Theorem 1 reduces to the usual DT, from which we have the following one-soliton solutions:

$$
\begin{aligned}
\widetilde{X}_n&=a_{n+1}^{(0)}X_n+b_{n+1}^{(0)}Y_n-c_{n+1}^{(1)},\\
\widetilde{Y}_n&=a_{n+1}^{(0)}Y_n-b_{n+1}^{(0)}X_n-d_{n+1}^{(1)},
\end{aligned}\tag{11}
$$

where $a_{n+1}^{(0)}$, $b_{n+1}^{(0)}$, $c_{n+1}^{(1)}$ and $d_{n+1}^{(1)}$ can be given by replacing n in $a_n^{(0)}$, $b_n^{(0)}$, $c_n^{(1)}$ and $d_n^{(1)}$ with $n+1$, in which $a_n^{(0)}=\frac{\Delta a_n^{(0)}}{\Delta_1^{\varepsilon(1)}}$, $b_n^{(0)}=\frac{\Delta b_n^{(0)}}{\Delta_1^{\varepsilon(1)}}$, $c_n^{(1)}=\frac{\Delta c_n^{(1)}}{\Delta_1^{\varepsilon(1)}}$ and $d_n^{(1)}=\frac{\Delta d_n^{(1)}}{\Delta_1^{\varepsilon(1)}}$ with

$$
\Delta_1^{\varepsilon(1)}=\begin{vmatrix}
\Psi_{1,n} & \Psi_{2,n} & -\lambda_1\Psi_{3,n} & -\lambda_1\Psi_{4,n}\\
\Psi_{2,n} & -\Psi_{1,n} & \lambda_1\Psi_{4,n} & -\lambda_1\Psi_{3,n}\\
\lambda_1^2\Psi_{3,n} & \lambda_1^2\Psi_{4,n} & \lambda_1\Psi_{1,n} & \lambda_1\Psi_{2,n}\\
\lambda_1^2\Psi_{4,n} & -\lambda_1^2\Psi_{3,n} & -\lambda_1\Psi_{2,n} & \lambda_1\Psi_{1,n}
\end{vmatrix},
$$

where $\Delta a_n^{(0)}$, $\Delta b_n^{(0)}$, $\Delta c_n^{(1)}$ and $\Delta d_n^{(1)}$ are obtained by replacing the first, second, third and final columns of $\Delta_1^{\varepsilon(1)}$ with column vector $(-\lambda_1^2\Psi_{1,n},-\lambda_1^2\Psi_{2,n},-\Psi_{3,n},-\Psi_{4,n})^{\mathrm{T}}$ separately. The solutions (11) can be rewritten as

$$
\begin{aligned}
\widetilde{X}_n&=-\frac{C_2C_4-C_1C_3}{C_1C_4+C_2C_3}\widetilde{Y}_n\\
&=\frac{(\lambda_1^4-1)(C_2C_4-C_1C_3)}{2\lambda_1^2\sqrt{(C_1^2+C_2^2)(C_3^2+C_4^2)}}\mathrm{sech}(\xi_1+\alpha),
\end{aligned}\tag{12}
$$

where $\xi_1=(2n+1)\ln\lambda_1+(\lambda_1^2-\frac{1}{\lambda_1^2})t$ and $\alpha=\frac{1}{2}\ln\frac{C_1^2+C_2^2}{C_3^2+C_4^2}$, with $\lambda_1>0$. Components $\widetilde{X}_n$ and $\widetilde{Y}_n$ are nonsingular and proportional. When C_i and λ_1 are taken as different values, we may give different shapes of one-soliton solutions, as listed in Table 1. As an example, in what follows we choose $C_1=C_3=-C_4=1$, $C_2=1/2$, $\lambda_1=2$, then the structures and some physical properties of one-soliton solutions are given in Fig. 1 and Table 2.

Figures 1(a) and 1(c) show the 3D structures of one-soliton solutions $\widetilde{X}_n$ and $\widetilde{Y}_n$, while Figs. 1(b) and 1(d) display the 2D structures of one-soliton solutions $\widetilde{X}_n$ and $\widetilde{Y}_n$, respectively. In addition, in order to analyze the dynamical behaviors of one-soliton solutions, we conduct numerical simulation through the finite difference method,[40] as shown in Fig. 2. Figures 2(a), 2(e) and 2(b), 2(f) are the exact and approximate one-soliton solutions without any noise. Figures 2(c), 2(g) and 2(d), 2(h) are the perturbed solutions with 2% and 5% noises, respectively. By the numerical simulation, the one-soliton solutions have small fluctuations in a short time when adding 2% noise. As the noise increases, the structures of one-soliton exhibit significant fluctuations.

Table 1. Relations between the parameters and shapes of one-soliton solutions. BS: bright soliton; ABS: anti-bell-shaped soliton.

Solitons	Parameters	Shapes
$\widetilde{X}_n$, $\widetilde{Y}_n$	$\lambda_1>1, C_2C_4-C_1C_3>0, C_1C_4+C_2C_3<0$ or $0<\lambda_1<1, C_2C_4-C_1C_3<0, C_1C_4+C_2C_3>0$	BS-BS
	$\lambda_1>1, C_2C_4-C_1C_3<0, C_1C_4+C_2C_3<0$ or $0<\lambda_1<1, C_2C_4-C_1C_3>0, C_1C_4+C_2C_3>0$	ABS-BS
	$\lambda_1>1, C_2C_4-C_1C_3>0, C_1C_4+C_2C_3>0$ or $0<\lambda_1<1, C_2C_4-C_1C_3<0, C_1C_4+C_2C_3<0$	BS-ABS

Table 2. Physical properties of one-soliton solutions. Energy of $\widetilde{X}_n$ and $\widetilde{Y}_n$ are given by $E_{\widetilde{X}_n}=\int_{-\infty}^{+\infty}\widetilde{X}_n^2\,\mathrm{d}n$ and $E_{\widetilde{Y}_n}=\int_{-\infty}^{+\infty}\widetilde{Y}_n^2\,\mathrm{d}n$.

Solitons	Amplitude	Velocity	Wave number	Width	Primary phase	Energy
$\widetilde{X}_n$	$\frac{\lvert(\lambda_1^4-1)(C_2C_4-C_1C_3)\rvert}{2\lambda_1^2\sqrt{(C_1^2+C_2^2)(C_3^2+C_4^2)}}$	$-\frac{\lambda_1^4-1}{2\lambda_1^2\ln\lambda_1}$	$2\ln\lambda_1$	$\frac{1}{2\ln\lambda_1}$	$\ln\lambda_1+\alpha$	$\frac{(\lambda_1^4-1)^2(C_2C_4-C_1C_3)^2}{4\lambda_1^4(C_1^2+C_2^2)(C_3^2+C_4^2)\lvert\ln\lambda_1\rvert}$
$\widetilde{Y}_n$	$\frac{\lvert(\lambda_1^4-1)(C_1C_4+C_2C_3)\rvert}{2\lambda_1^2\sqrt{(C_1^2+C_2^2)(C_3^2+C_4^2)}}$	$-\frac{\lambda_1^4-1}{2\lambda_1^2\ln\lambda_1}$	$2\ln\lambda_1$	$\frac{1}{2\ln\lambda_1}$	$\ln\lambda_1+\alpha$	$\frac{(\lambda_1^4-1)^2(C_1C_4+C_2C_3)^2}{4\lambda_1^4(C_1^2+C_2^2)(C_3^2+C_4^2)\lvert\ln\lambda_1\rvert}$

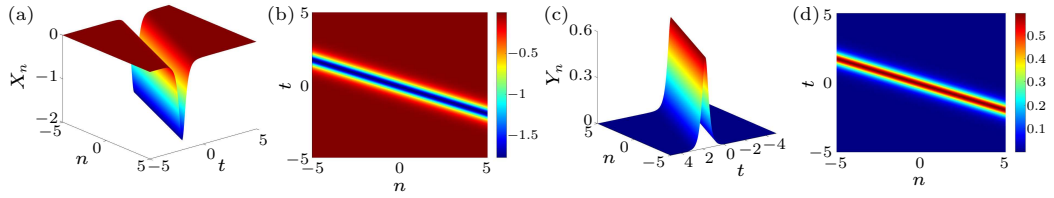


Fig. 1. One-soliton solutions: [(a), (b)] the component $\widetilde{X}_n$; [(c), (d)] the component $\widetilde{Y}_n$.

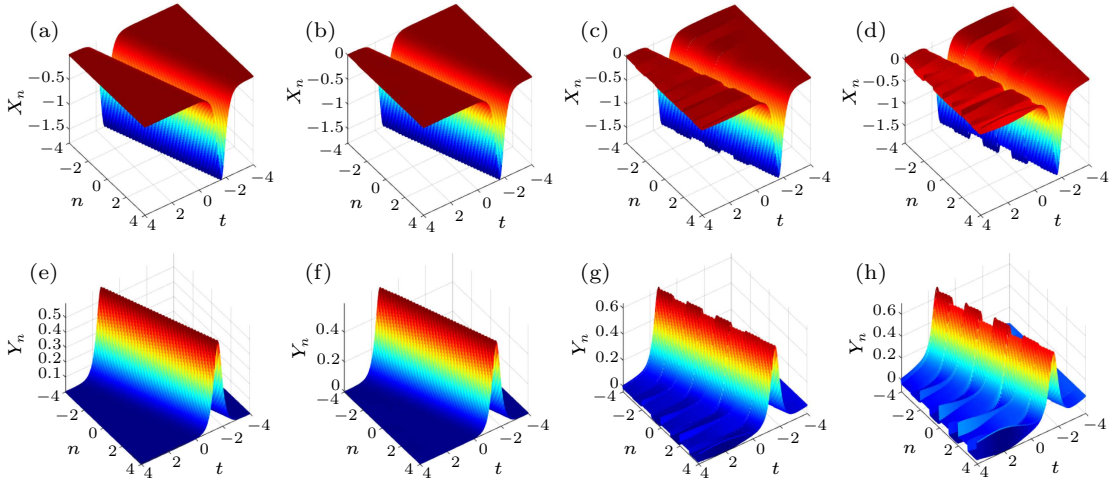


Fig. 2. One-soliton solutions: [(a), (e)] exact solutions; [(b), (f)] perturbed solutions without noise; [(c), (g)] perturbed solutions with 2% noise; [(d), (h)] perturbed solutions with 5% noise.

When $N=r=2$ and Taylor expansions are not performed on spectral parameters λ_1 and λ_2, by choosing $C_1=C_3=-C_4=1$, $C_2=1/2$ and employing the generalized $(2,0)$-fold DT, the exact two-soliton solutions are arrived at

$$\widetilde{X}_n=-3\widetilde{Y}_n=\frac{3\sqrt{10}(\lambda_1^2\lambda_2^2-1)(\lambda_1^2-\lambda_2^2)[\lambda_1^2(1-\lambda_2^4)\cosh(\xi_1+\alpha)+\lambda_2^2(\lambda_1^4-1)\cosh(\xi_2+\alpha)]}{10\lambda_1^2\lambda_2^2[(\lambda_1^2-\lambda_2^2)^2\cosh(\xi_1+\xi_2+2\alpha)+(\lambda_1^2\lambda_2^2-1)^2\cosh(\xi_1-\xi_2)+(\lambda_1^4-1)(1-\lambda_2^4)]},\tag{13}$$

where $\xi_i=(2n+1)\ln\lambda_i+(\lambda_i^2-\frac{1}{\lambda_i^2})t$ $(\lambda_i>0,\ i=1,\ 2)$ and $\alpha=\frac{1}{2}(\ln5-3\ln2)$. Now we will make the asymptotic analysis of two-soliton solutions, and their physical properties are listed in Table 3.

Before the collision ($t \to -\infty$):

$$\begin{aligned}
&\xi_1 \sim 0,\ \xi_2 \to -\infty: \quad \widetilde{X}_n \longrightarrow \widetilde{X}^-_{1,n} = \frac{3\sqrt{10}(\lambda_1^4-1)}{20\lambda_1^2}\mathrm{sech}(\xi_1+\alpha+\ln|\frac{\lambda_1^2\lambda_2^2-1}{\lambda_1^2-\lambda_2^2}|),\ \widetilde{Y}_n \longrightarrow -\frac{1}{3}\widetilde{X}^-_{1,n},\\
&\xi_2 \sim 0,\ \xi_1 \to -\infty: \quad \widetilde{X}_n \longrightarrow \widetilde{X}^-_{2,n} = \frac{3\sqrt{10}(1-\lambda_2^4)}{20\lambda_2^2}\mathrm{sech}(\xi_2+\alpha+\ln|\frac{\lambda_1^2\lambda_2^2-1}{\lambda_1^2-\lambda_2^2}|),\ \widetilde{Y}_n \longrightarrow -\frac{1}{3}\widetilde{X}^-_{2,n},
\end{aligned} \tag{14}$$

where $\widetilde{X}^-_{i,n}$ $(i=1,\ 2)$ are the limit states before two solitons collide with each other.

After the collision ($t \to +\infty$):

$$\begin{aligned}
&\xi_1 \sim 0,\ \xi_2 \to +\infty: \quad \widetilde{X}_n \longrightarrow \widetilde{X}^+_{1,n} = \frac{3\sqrt{10}(\lambda_1^4-1)}{20\lambda_1^2}\mathrm{sech}(\xi_1+\alpha-\ln|\frac{\lambda_1^2\lambda_2^2-1}{\lambda_1^2-\lambda_2^2}|),\ \widetilde{Y}_n \longrightarrow -\frac{1}{3}X^+_{1,n},\\
&\xi_2 \sim 0,\ \xi_1 \to +\infty: \quad \widetilde{X}_n \longrightarrow \widetilde{X}^+_{2,n} = \frac{3\sqrt{10}(1-\lambda_2^4)}{20\lambda_2^2}\mathrm{sech}(\xi_2+\alpha-\ln|\frac{\lambda_1^2\lambda_2^2-1}{\lambda_1^2-\lambda_2^2}|),\ \widetilde{Y}_n \longrightarrow -\frac{1}{3}X^+_{2,n},
\end{aligned} \tag{15}$$

where $\widetilde{X}^+_{i,z}$ $(i=1,\ 2)$ are the limit states after two solitons collide with each other.

Table 3. Physical properties of two-soliton solutions.

Solitons	Amplitude	Velocity	Wave number	Width	Primary phase	Energy
$\widetilde{X}^-_{1,n}$	$\frac{3\sqrt{10}(\lambda_1^4-1)}{20\lambda_1^2}$	$-\frac{\lambda_1^4-1}{2\lambda_1^2\ln\lambda_1}$	$2\ln\lambda_1$	$\frac{1}{2\ln\lambda_1}$	$\ln\lvert\frac{\lambda_1(\lambda_1^2\lambda_2^2-1)}{\lambda_1^2-\lambda_2^2}\rvert+\alpha$	$\frac{9(\lambda_1^4-1)^2}{40\lambda_1^4\lvert\ln\lambda_1\rvert}$
$\widetilde{X}^-_{2,n}$	$\frac{3\sqrt{10}(1-\lambda_2^4)}{20\lambda_2^2}$	$-\frac{\lambda_2^4-1}{2\lambda_2^2\ln\lambda_2}$	$2\ln\lambda_2$	$\frac{1}{2\ln\lambda_2}$	$\ln\lvert\frac{\lambda_2(\lambda_1^2\lambda_2^2-1)}{\lambda_1^2-\lambda_2^2}\rvert+\alpha$	$\frac{9(1-\lambda_2^4)^2}{40\lambda_2^4\lvert\ln\lambda_2\rvert}$
$\widetilde{X}^+_{1,n}$	$\frac{3\sqrt{10}(\lambda_1^4-1)}{20\lambda_1^2}$	$-\frac{\lambda_1^4-1}{2\lambda_1^2\ln\lambda_1}$	$2\ln\lambda_1$	$\frac{1}{2\ln\lambda_1}$	$\ln\lvert\frac{\lambda_1(\lambda_1^2-\lambda_2^2)}{\lambda_1^2\lambda_2^2-1}\rvert+\alpha$	$\frac{9(\lambda_1^4-1)^2}{40\lambda_1^4\lvert\ln\lambda_1\rvert}$
$\widetilde{X}^+_{2,n}$	$\frac{3\sqrt{10}(1-\lambda_2^4)}{20\lambda_2^2}$	$-\frac{\lambda_2^4-1}{2\lambda_2^2\ln\lambda_2}$	$2\ln\lambda_2$	$\frac{1}{2\ln\lambda_2}$	$\ln\lvert\frac{\lambda_2(\lambda_1^2-\lambda_2^2)}{\lambda_1^2\lambda_2^2-1}\rvert+\alpha$	$\frac{9(1-\lambda_2^4)^2}{40\lambda_2^4\lvert\ln\lambda_2\rvert}$

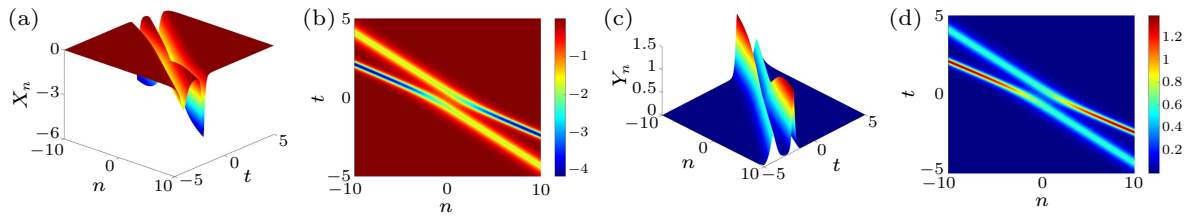


Fig. 3. Two-soliton solutions: [(a), (b)] the component $\widetilde{X}_z$; [(c), (d)] the component $\widetilde{Y}_z$.

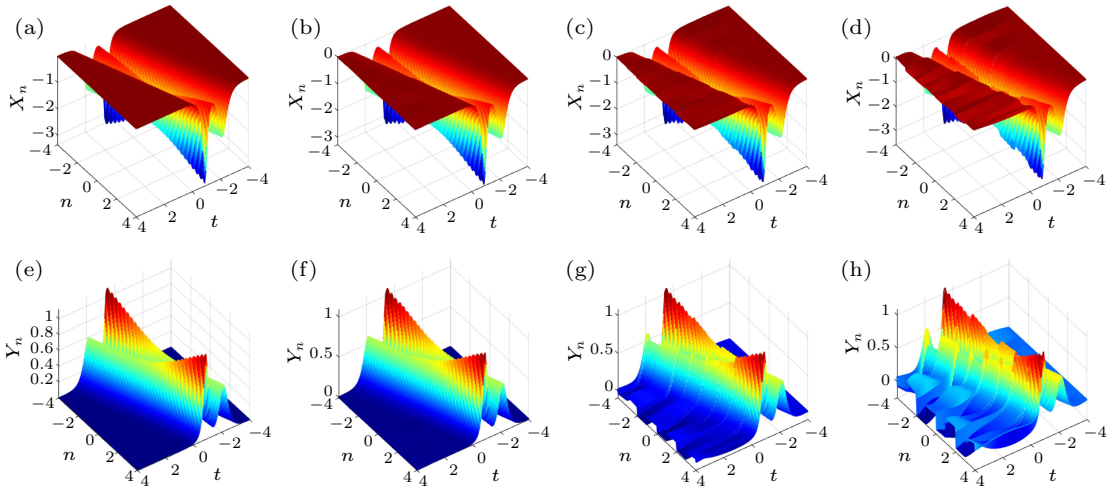


Fig. 4. Two-soliton solutions: [(a), (e)] exact solutions; [(b), (f)] perturbed solutions without noise; [(c), (g)] perturbed solutions with 2% noise; [(d), (h)] perturbed solutions with 5% noise.

From Eqs. (14), (15) and Table 3, we can conclude that the amplitude and velocity of solitons keep unaltered before and after the collision, but their phases are changed. The two-soliton solutions with spectral parameters $\lambda_1 = 2$ and $\lambda_2 = 1/3$ are drawn in Fig. 3. Figures 3(a), 3(c) and 3(b), 3(d) display the 3D and 2D structures of two-soliton solutions re-

spectively. Figure 4 exhibits the numerical simulation of two-soliton. Specifically, Figs. 4(a) and 4(e) are the explicit two-soliton solutions, Figs. 4(b) and 4(f) are the perturbed solutions without noise, and Figs. 4(c), 4(g) and 4(d), 4(h) are the solutions with 2% and 5% noises, respectively. From Fig. 4, we know easily that the two-soliton solutions can only resist minor noise, but when the noise exceeds 5%, they will exhibit significant fluctuations.

When $N=r=3$ and Taylor expansions are not performed on spectral parameters λ_1, λ_2 and λ_3, Theorem 1 degenerates into the $(3,0)$-fold DT, from which we can obtain the three-soliton solutions with the parameters $C_1=C_3=-C_4=1$, $C_2=1/2$. The structures of three-soliton solutions with spectral parameters $\lambda_1=2$, $\lambda_2=1/3$ and $\lambda_3=7/3$ are displayed in Fig. 5. Figures 5(a) and 5(c) display the 3D structures of three-soliton solutions $\widetilde{X}_n$ and $\widetilde{Y}_n$. Figures 5(b) and 5(d) show the 2D structures of $\widetilde{X}_n$ and $\widetilde{Y}_n$, respectively.

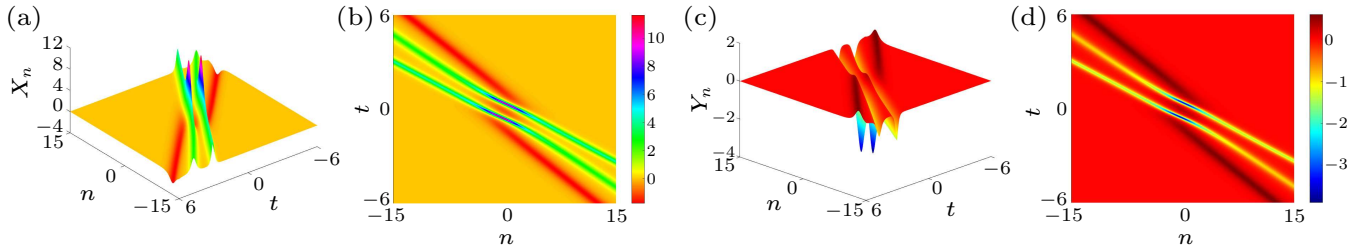


Fig. 5. Three-soliton solutions: [(a), (b)] the component $\widetilde{X}_n$; [(c), (d)]the component $\widetilde{Y}_n$.

3.1.2. Higher-order SRS solutions

When using the generalized $(1,N-1)$-fold DT and choosing the parameters $C_1=C_3=-C_4=1$, $C_2=1/2$, we can obtain some higher-order SRS solutions. Firstly, taking the spectral parameter $\lambda_1=2$ and expand Ψ_n into the Taylor series with $\lambda=\lambda_1+\varepsilon^2$ at $\varepsilon=0$:

$$\begin{aligned}\Psi_n(\lambda_1+\varepsilon^2)&=\sum_{j=0}^{\infty}\Psi_n^{(j)}\varepsilon^{2j}\\&=\Psi_n^{(0)}+\Psi_n^{(1)}\varepsilon^2+\Psi_n^{(2)}\varepsilon^4+\Psi_n^{(3)}\varepsilon^6+\cdots,\end{aligned}\tag{16}$$

where the first two coefficient vectors are given as

$$\Psi_n^{(0)}=\begin{pmatrix}\Psi_{1,n}^{(0)}\\ \Psi_{2,n}^{(0)}\\ \Psi_{3,n}^{(0)}\\ \Psi_{4,n}^{(0)}\end{pmatrix}=\begin{pmatrix}2^n\mathrm{e}^{4t+2e_0}\\ 2^{-1+n}\mathrm{e}^{4t+2e_0}\\ 2^{-n}\mathrm{e}^{\frac{1}{4}t-2e_0}\\ -2^{-n}\mathrm{e}^{\frac{1}{4}t-2e_0}\end{pmatrix},$$

$$\Psi_n^{(1)}=\begin{pmatrix}\mathrm{e}^{4t+2e_0}(4t+2e_1+\frac{1}{2}n)2^n\\ \frac{1}{4}\mathrm{e}^{4t+2e_0}(4e_1+n+8t)2^n\\ -\frac{1}{4}\mathrm{e}^{\frac{1}{4}t-2e_0}(t+8e_1+2n)2^{-n}\\ \frac{1}{4}\mathrm{e}^{\frac{1}{4}t-2e_0}(t+8e_1+2n)2^{-n}\end{pmatrix}.$$

When $N=1$ and using the above expressions, we can get the first-order SRS solutions as follows:

$$\begin{aligned}\widetilde{X}_n&=a_{n+1}^{(0)}X_n+b_{n+1}^{(0)}Y_n-c_{n+1}^{(1)},\\ \widetilde{Y}_n&=a_{n+1}^{(0)}Y_n-b_{n+1}^{(0)}X_n-d_{n+1}^{(1)},\end{aligned}\tag{17}$$

where $a_{n+1}^{(0)}$, $b_{n+1}^{(0)}$, $c_{n+1}^{(1)}$ and $d_{n+1}^{(1)}$ can be given by replacing n in $a_n^{(0)}$, $b_n^{(0)}$, $c_n^{(1)}$ and $d_n^{(1)}$ with $n+1$, in which $a_n^{(0)}=\frac{\Delta a_n^{(0)}}{\Delta_1^{\varepsilon(1)}}$, $b_n^{(0)}=\frac{\Delta b_n^{(0)}}{\Delta_1^{\varepsilon(1)}}$, $c_n^{(1)}=\frac{\Delta c_n^{(1)}}{\Delta_1^{\varepsilon(1)}}$ and $d_n^{(1)}=\frac{\Delta d_n^{(1)}}{\Delta_1^{\varepsilon(1)}}$ with

$$\Delta_1^{\varepsilon(1)}=\begin{vmatrix}\Psi_{1,n}^{(0)} & \Psi_{2,n}^{(0)} & -\lambda_1\Psi_{3,n}^{(0)} & -\lambda_1\Psi_{4,n}^{(0)}\\ \Psi_{2,n}^{(0)} & -\Psi_{1,n}^{(0)} & \lambda_1\Psi_{4,n}^{(0)} & -\lambda_1\Psi_{3,n}^{(0)}\\ \lambda_1^2\Psi_{3,n}^{(0)} & \lambda_1^2\Psi_{4,n}^{(0)} & \lambda_1\Psi_{1,n}^{(0)} & \lambda_1\Psi_{2,n}^{(0)}\\ \lambda_1^2\Psi_{4,n}^{(0)} & -\lambda_1^2\Psi_{3,n}^{(0)} & -\lambda_1\Psi_{2,n}^{(0)} & \lambda_1\Psi_{1,n}^{(0)}\end{vmatrix},$$

and $\Delta a_n^{(0)}$, $\Delta b_n^{(0)}$, $\Delta c_n^{(1)}$ and $\Delta d_n^{(1)}$ can be obtained by replacing the first, second, third and fourth columns of $\Delta_1^{\varepsilon(1)}$ with $(-\lambda_1^2\Psi_{1,n}^{(0)},-\lambda_1^2\Psi_{2,n}^{(0)},-\Psi_{3,n}^{(0)},-\Psi_{4,n}^{(0)})^{\mathrm{T}}$ respectively. The exact first-order RS solutions (17) can also be rewritten as

$$\widetilde{X}_n=-3\widetilde{Y}_n=-\frac{2^{2n-\frac{5}{2}}45\cosh\mu_1}{(\sqrt{5})^{n-1}(\cosh\mu_2+10)},\tag{18}$$

where $\mu_1=2n\ln 2+\frac{1}{2}\ln 5+\frac{15}{4}t+4e_0$ and $\mu_2=(2n-1)\ln 2+\frac{n}{2}\ln 5+\frac{15}{2}t+8e_0$. The structures of the first-order SRS solutions are shown in Fig. 6. From the perspective of geometry, there seems to be no distinction between the one-soliton and first-order SRS at first glance. Actually, upon closer examination of solutions (12) and (18), it becomes evident that their analytic expressions differ. Furthermore, by adjusting the parameter e_0, we have the ability to manipulate the location of the SRS. Upon analyzing Fig. 6, it is obvious that the locations of the first-order SRS solutions have experienced substantial alterations.

When $N=2$, we can also obtain the second-order SRS solutions by Eq. (8), whose structures are displayed in Fig. 7. It should be noted that the second-order SRS solutions includes the exponential and polynomial function, which are different from the two-soliton solutions with only exponential function.

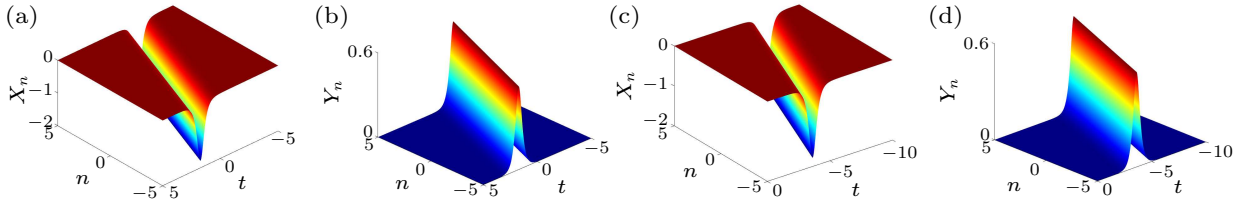


Fig. 6. First-order SRS: [(a), (b)] $e_0 = 0$, [(b), (d)] $e_0 = 5$.

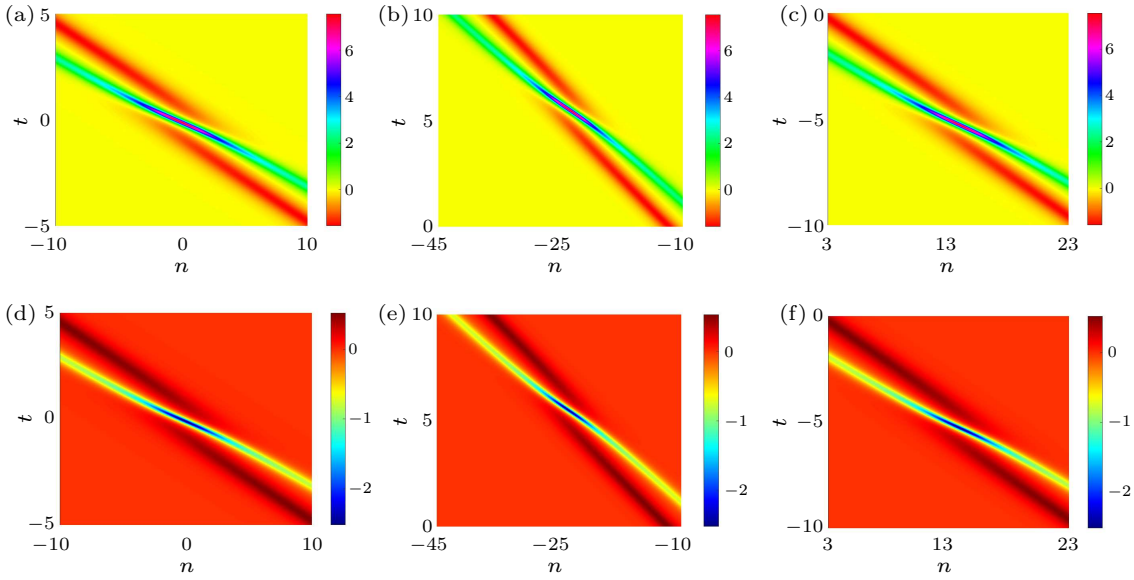


Fig. 7. Second-order SRS: [(a), (d)] $e_0 = e_1 = 0$; [(b), (e)] $e_0 = 3,\ e_1 = 0$; [(c), (f)] $e_0 = 0,\ e_1 = 2$.

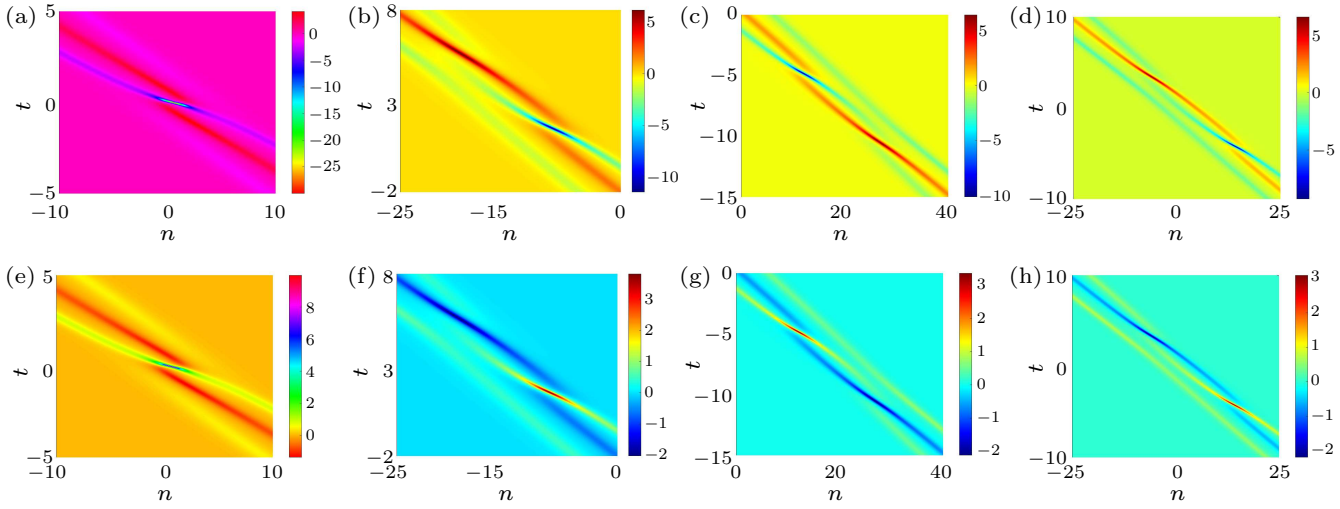


Fig. 8. Third-order SRS: [(a), (e)] $e_0 = e_1 = e_2 = 0$; [(b), (f)] $e_0 = 2,\ e_1 = e_2 = 0$; [(c), (g)] $e_1 = 3,\ e_0 = e_2 = 0$; [(b), (f)] $e_2 = 5,\ e_0 = e_1 = 0$.

From Fig. 7, it is obvious that both parameters e_0 and e_1 have an impact on the position of the second-order SRS solutions interact.

When $N = 3$, the structures of the third-order SRS solutions are shown in Fig. 8. Similar to the second-order SRS solutions, the third-order SRS solutions also comprises three controlling parameters: e_0, e_1 and e_2. These parameters solely govern the position of these SRSs in interaction but they cannot be individually separated.

3.2. Higher-order RS solutions on the non-vanishing background

In this subsection, we select the nonzero seed solutions $X_n = a$, $Y_n = b$ and substitute them into Eq. (3) to obtain the following fundamental solution:

$$\Psi_n = \begin{pmatrix} \Psi_{1,n} \\ \Psi_{2,n} \\ \Psi_{3,n} \\ \Psi_{4,n} \end{pmatrix} = \begin{pmatrix} M_1 \\ M_3 \\ (M_1 a + M_3 b)\frac{\tau_+ - \lambda}{a^2+b^2} \\ (M_1 b - M_3 a)\frac{\tau_+ - \lambda}{a^2+b^2} \end{pmatrix} \tau_+^n \mathrm{e}^{\rho_+ t + \delta(\varepsilon)}$$

$$+\begin{pmatrix} M_2 \\ M_4 \\ (M_2a+M_4b)\frac{\tau_--\lambda}{a^2+b^2} \\ (M_2b-M_4a)\frac{\tau_--\lambda}{a^2+b^2} \end{pmatrix}\tau_-^n e^{\rho_- t-\delta(\varepsilon)}, \tag{19}$$

where $\beta=\sqrt{\lambda^4-4(a^2+b^2)\lambda^2-2\lambda^2+1}$, $\tau_\pm=\frac{1}{2\lambda}(\lambda^2+1\pm\beta)$, $\rho_\pm=(\lambda+\frac{1}{\lambda})\tau_\pm+a^2+b^2-1$, $\delta(\varepsilon)=\beta\Sigma_{k=0}^{\infty}e_k\varepsilon^{2k}$, with e_k, M_1, M_2, M_3 and M_4 being arbitrary constants and $\varepsilon\ll 1$. For Eq. (19), we can consider the RS solutions based on three types of seed solutions, namely: (i) $a\neq 0$, $b=0$; (ii) $a=0$, $b\neq 0$; (iii) $a\neq 0$, $b\neq 0$. Interestingly, the RS structures of (i) and (ii) are exchanged. The RS structures of case (iii) and the first two cases (i), (ii) are similar, except that their backgrounds have changed. Thus, as a special example, here we only analyze case (i).

The first step to obtaining rational solutions is to choose $\lambda=\lambda_1+\varepsilon^2$ with $\lambda_1=a+\sqrt{a^2+1}$ and expand the fundamental solution (19) into Taylor series around $\varepsilon=0$. Without loss of generality, choosing $M_1=M_2=1$, $M_3=-M_4=\frac{1}{\varepsilon}$, $a=\frac{3}{4}$ (i.e., $\lambda_1=2$), we can expand Ψ_n into the form similar to Eq. (16). Here the first two coefficient vectors are given by

$$\Psi_n^{(0)}=\begin{pmatrix}\Psi_{1,n}^{(0)}\\ \Psi_{2,n}^{(0)}\\ \Psi_{3,n}^{(0)}\\ \Psi_{4,n}^{(0)}\end{pmatrix}=\left(\frac{5}{4}\right)^n e^{\frac{43}{16}t}\begin{pmatrix}2\\ \frac{\sqrt{15}}{20}(s+40e_0)\\ -2\\ \frac{3\sqrt{15}}{20}(s+40e_0-\frac{40}{3})\end{pmatrix},$$

$$\Psi_n^{(1)}=(\frac{5}{4})^n e^{\frac{43}{16}t}\begin{pmatrix}\Psi_{1,n}^{(1)}\\ \Psi_{2,n}^{(1)}\\ \Psi_{3,n}^{(1)}\\ \Psi_{4,n}^{(1)}\end{pmatrix},$$

in which $s=8n+25t$ and

$$\Psi_{1,n}^{(1)}=\frac{3}{320}s^2+\frac{3}{4}e_0s+\frac{15}{4}t+15e_0^2,$$

$$\Psi_{2,n}^{(1)}=\frac{\sqrt{15}}{38400}[3s^3+360e_0s^2+(14400e_0^2+3600t+112)s+(144000e_0+19200)t+192000e_0^3+50560e_0+76800e_1],$$

$$\Psi_{3,n}^{(1)}=-\frac{3}{320}s^2-\frac{1}{4}(3e_0-1)s-15e_0^2+10e_0-\frac{15}{4}t-\frac{5}{3},$$

$$\Psi_{4,n}^{(1)}=\frac{\sqrt{15}}{115200}[9s^3+(1080e_0-360)s^2+(43200e_0^2-28800e_0+10800t+5136)s+(432000e_0-86400)t+576000e_0^3-576000e_0^2+343680e_0+230400e_1-12160].$$

If expand Ψ_n at $\lambda_1\neq 2$ into Taylor series, we can also derive the SRS on the non-vanishing background via the discrete generalized $(1,N-1)$-fold DT. In the following, we will apply the discrete generalized $(1,N-1)$-fold DT and utilize the above expansions to obtain higher-order RS solutions of Eq. (2).

3.2.1. First-order RS solutions

When $N=1$ and employing the generalized $(1,0)$-fold DT, we can give the first-order RS solutions by Eq. (17), which can be expressed explicitly as

$$\widetilde{X}_n=\frac{3}{4}-\frac{1200}{9(s+40e_0-\frac{8}{3})^2+1216},$$
$$\widetilde{Y}_n=\frac{480\sqrt{15}}{9(s+40e_0-\frac{8}{3})^2+1216}, \tag{20}$$

from which we have the following conclusions:

When $n\to\pm\infty$ or $t\to\pm\infty$, the first-order RS solutions $\widetilde{X}_n$ and $\widetilde{Y}_n$ reduce to their seed backgrounds, namely $\widetilde{X}_n\to\frac{3}{4}$ and $\widetilde{Y}_n\to 0$.

It is obvious that the valley of $\widetilde{X}_n$ and the peak of $\widetilde{Y}_n$ are located on the straight line $s+40e_0-\frac{8}{3}=0$, where e_0 is the parameter that can control the positions of the peak and valley. On the straight line $s+40e_0-\frac{8}{3}=0$, $\widetilde{X}_n$ reaches the minimum $-9/38$ and $\widetilde{Y}_n$ reaches the maximum $15\sqrt{15}/38$.

The velocity, wave number, width and primary phase of Eq. (20) are $-\frac{25}{8}$, 8, $\frac{1}{8}$, and $40e_0-\frac{8}{3}$, respectivley.

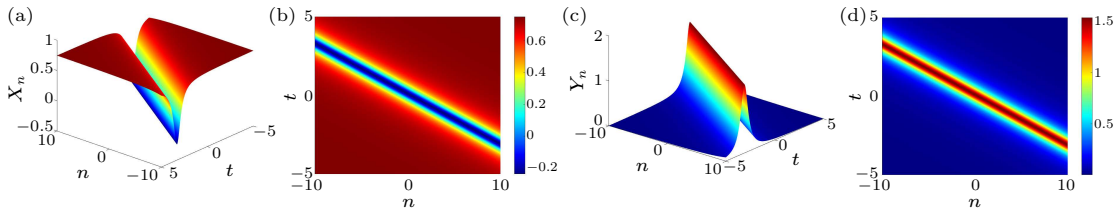


Fig. 9. First-order RS solutions with $e_0=0$: [(a), (b)] the component $\widetilde{X}_n$; [(c), (d)] the component $\widetilde{Y}_n$.

The structures of Eq. (20) are shown in Fig. 9. Figures 9(a) and 9(c) are the 3D structures of $\widetilde{X}_n$ and $\widetilde{Y}_n$, respectively, and Figs. 9(b) and 9(d) are the 2D structures of $\widetilde{X}_n$ and $\widetilde{Y}_n$, respectively. Comparing Figs. 2 and 9, there seems to be no difference in appearance between the usual soliton and RS, except for their different seed backgrounds. In fact, there is a notable contrast in the expressions of these two types of solutions. The usual soliton solutions usually contain exponential function or hyperbolic function, while the RS solutions only consist of rational expressions.

Like the one-soliton solutions, we perform the numerical simulation on the first-order RS solutions, as shown in

Fig. 10. Figures 10(a) and 10(e) show the exact first-order RS solutions. Figures 10(b) and 10(f) are the perturbed solutions with no noise. Figures 10(c), 10(g) and 10(d), 10(h) exhibit the solutions with 2% and 10% noises, respectively. From Fig. 10, it can be seen that the first-order RS has a small fluctuation when noise is not greater than 2%, whereas the structures of first-order RS may have visible fluctuations if the noise is greater than 2%, such as noise = 10% (see Figs. 10(d) and 10(h)). Therefore, we can conclude that the first-order RS can resist very small noise.

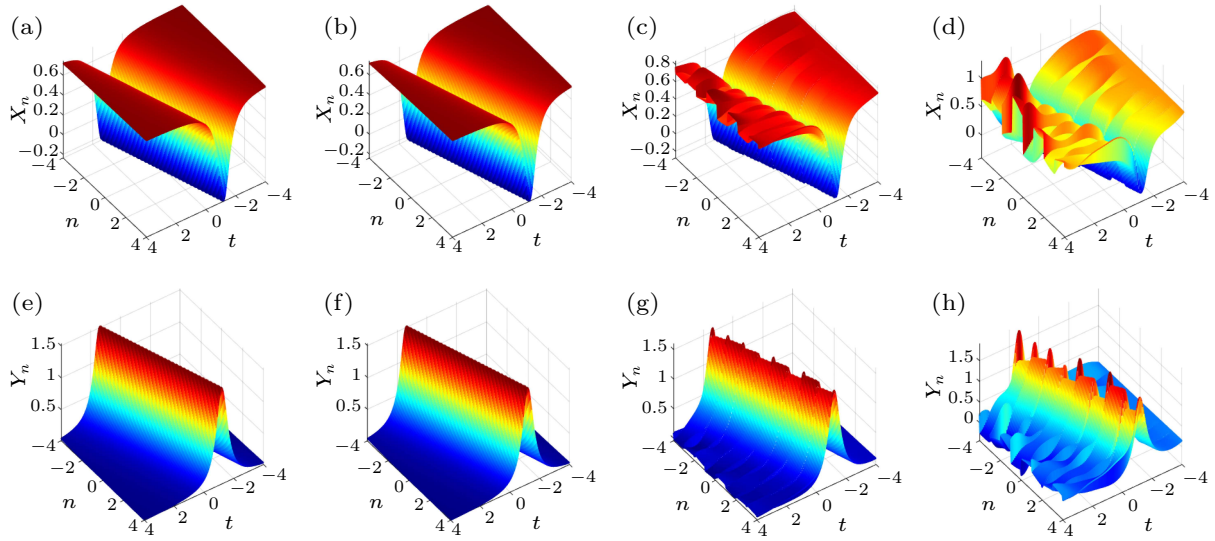


Fig. 10. First-order RS solutions with $e_0 = 0$: [(a), (e)] exact solutions; [(b), (f)] perturbed solutions without noise; [(c), (g)] perturbed solutions with 2% noise; [(d), (h)] perturbed solutions with 10% noise.

3.2.2. Second-order RS solutions

When $N = 2$ and using the generalized $(1,1)$-fold DT, we can give the second-order RS solutions by

$$\widetilde{X}_n = a^{(0)}_{n+1} X_n + b^{(0)}_{n+1} Y_n - c^{(3)}_{n+1},$$
$$\widetilde{Y}_n = a^{(0)}_{n+1} Y_n - b^{(0)}_{n+1} X_n - d^{(3)}_{n+1},$$

which can be explicitly expressed as

$$\widetilde{X}_n = \frac{3}{4} - \frac{3600F_1}{G_1}, \quad \widetilde{Y}_n = \frac{1440\sqrt{15}F_2}{G_1}, \tag{21}$$

where

$$\begin{aligned}
F_1 =& 9s^4 + (1440e_0 - 96)s^3 + (86400e_0^2 - 11520e_0 \\
&+ 7104)s^2 + (2304000e_0^3 - 460800e_0^2 + 706560e_0 \\
&+ 230400e1 + 57600t - 29696)s + (2304000e_0 \\
&- 153600)t + 23040000e_0^4 - 6144000e_0^3 + 16896000e_0^2 \\
&+ 9216000e_0e1 - 1556480e_0 - 614400e_1 + 332800, \\
G_1 =& 81s^6 + (19440e_0 - 1296)s^5 + (1944000e_0^2 - 259200e_0 \\
&+ 31104)s^4 + (103680000e_0^3 - 20736000e_0^2 \\
&+ 3732480e_0 - 2073600e_1 - 518400t - 331776)s^3 \\
&+ [(-62208000e_0 + 4147200)t + 3110400000e_0^4 \\
&- 829440000e_0^3 + 149299200e_0^2 - 248832000e_0e_1 \\
&- 29859840e_0 + 16588800e_1 + 18183168]s^2 \\
&+ [(-2488320000e_0^2 + 331776000e_0 + 232243200)t \\
&+ 49766400000e_0^5 - 16588800000e_0^4 + 1990656000e_0^3 \\
&- 9953280000e_0^2e_1 - 796262400e_0^2 + 1327104000e_0e_1 \\
&+ 2012037120e_0 + 928972800e_1 - 63160320]s \\
&+ 829440000t^2 + (-33177600000e_0^3 + 6635520000e_0^2 \\
&+ 13271040000e_0 + 6635520000e_1 - 442368000)t \\
&+ 331776000000e_0^6 - 132710400000e_0^5 \\
&- 132710400000e_0^3e_1 - 5308416000e_0^3 \\
&+ 26542080000e_0^2e_1 + 56165990400e_0^2 \\
&+ 53084160000e_0e_1 + 13271040000e_1^2 \\
&- 3588096000e_0 - 1769472000e_1 + 581693440, \\
F_2 =& 9s^4 + (1440e_0 - 96)s^3 + (86400e_0^2 - 11520e_0 + 2280)s^2 \\
&+ (2304000e_0^3 - 460800e_0^2 + 320640e_0 + 230400e_1 \\
&+ 57600t - 3968)s + (2304000e_0 - 153600)t \\
&+ 23040000e_0^4 - 6144000e_0^3 + 9177600e_0^2 \\
&+ 9216000e_0e_1 - 527360e_0 - 614400e_1 - 353280.
\end{aligned}$$

For solutions (21), we can perform asymptotic analysis to discuss the limit behaviors of the second-order RS $\widetilde{X}_n$ and $\widetilde{Y}_n$. First of all, letting $\eta_1 = s - (3200t)^{\frac{1}{3}}$, the limit states of solutions (21) when $t \to \pm\infty$ can be expressed as

$$\widetilde{X}_n \longrightarrow \widetilde{X}^{\pm}_{1,n} = \frac{3}{4} - \frac{1200}{(3\eta_1 - 8 + 120e_0)^2 + 1216},$$
$$\widetilde{Y}_n \longrightarrow \widetilde{Y}^{\pm}_{1,n} = \frac{480\sqrt{15}}{(3\eta_1 - 8 + 120e_0)^2 + 1216}. \tag{22}$$

Along the curve $3\eta_1 - 8 + 120e_0 = 0$, the limit state of $\widetilde{X}_n$ reaches the minimum $-9/38$ and the limit state of $\widetilde{Y}_n$ reaches maximum $15\sqrt{15}/38$. The 3D structures of the second-order

RS are shown in Fig. 11, from which we can find that their positions of interaction have been changed obviously under the effect of e_1.

The numerical simulations of solutions (21) are shown in Fig. 12. Figures 12(a), 12(e) and 12(b), 12(f) exhibit the exact solutions and perturbed solutions without noises, respectively. They are almost the same. This indicates that our numerical algorithm is correct, in other words, the wave propagations of solutions (21) are stable in the absence of noise. Figures 12(c), 12(g) and Figures 12(d), 12(h) are the numerical structures when adding 2% and 4% noises, respectively. As seen in Fig. 12, the structures of solutions (21) have minor fluctuation with the noise not more than 4% in the range of $t \in (-5,\ 5)$.

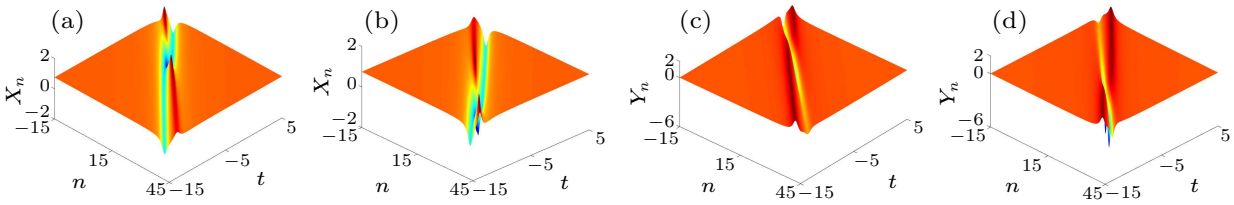


Fig. 11. Second-order RS solutions: [(a), (c)] $e_0 = e_1 = 0$; [(b), (d)] $e_0 = 0,\ e_1 = 2$.

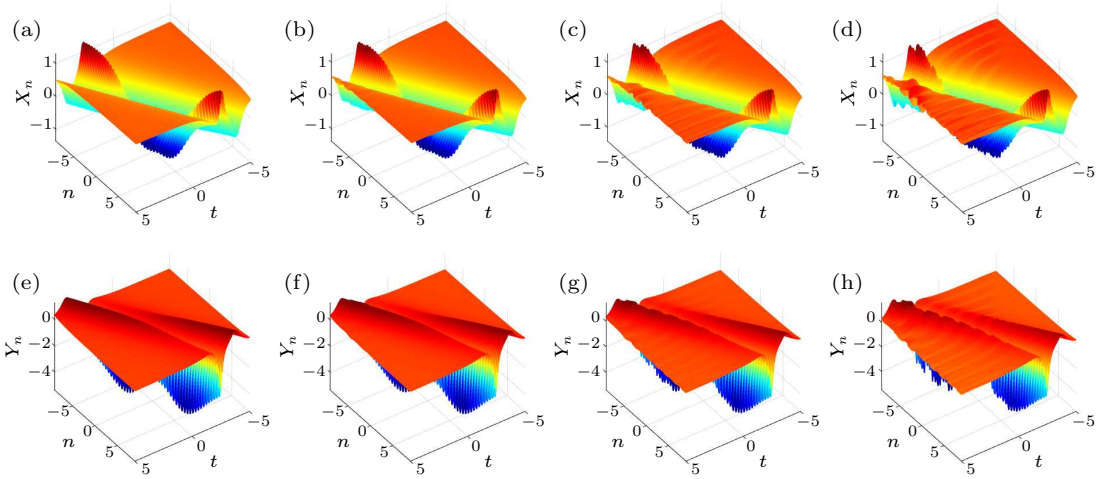


Fig. 12. Second-order RS solutions in Figs. 11(a) and 11(c): [(a), (e)] exact solutions; [(b), (f)] perturbed solutions without noise; [(c), (g)] perturbed solutions with 2% noise; [(d), (h)] perturbed solutions with 4% noise.

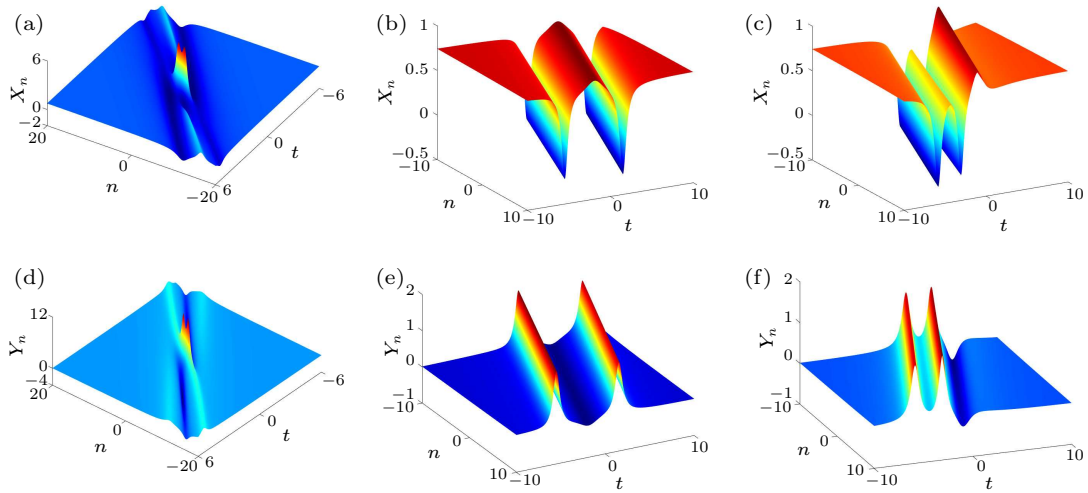


Fig. 13. Third-order RS solutions: [(a), (d)] $e_0 = e_1 = e_2 = 0$; [(b), (e)] $e_0 = e_2 = 0,\ e_1 = 20$; [(c), (f)] $e_0 = e_1 = 0,\ e_2 = 50$.

3.2.3. Third-order RS solutions

When $N = 3$ and using the generalized $(1,2)$-fold DT, we can obtain the third-order RS solutions, whose structures are shown in Fig. 13.

Figures 13(a) and 13(d) display the strong interaction of third-order RS solutions. In Figs. 13(b) and 13(e), under the effect of e_1, the component $\widetilde{X}_n$ is shown as three almost parallel RSs in the ranges of $n \in (-10,\ 10)$ and $t \in (-10,\ 10)$, where

the anti-dark RS appears between two dark RSs. In Fig. 13(e), due to the effect of e_1, the component $\widetilde{Y}_n$ is also shown as three almost parallel RSs in the ranges of $n \in (-10,\ 10)$ and $t \in (-10,\ 10)$, where the anti-bell shaped RS occurs between two bright RSs. However, they are actually not parallel, and within a certain range, there still exists interaction among three RSs. Figure 13(c) exhibits that the anti-dark RS lies on the right side of two dark RSs, while Fig. 13(f) shows that the anti-bell shaped RS is located on the right side of two bright RSs. However, when the coordinate axis range is large enough, there still exist interactions among these RSs like the second-order RS.

3.3. Mixed hyperbolic-rational soliton solutions on non-vanishing background

When $N = r = 2$ and using the generalized $(2,0)$-fold DT, we will obtain the mixed solutions of the usual soliton (US) and RS, which are also called the mixed hyperbolic-rational soliton solutions. At this point, we need to use two spectral parameters λ_1 and λ_2. For λ_1, we choose the corresponding parameters as $M_1 = M_2 = 1$, $M_3 = -M_4 = 1/\varepsilon$, $a = 3/4$, $\lambda_1 = 2$, while for λ_2, we choose the corresponding parameters as $M_1 = M_3 = -M_4 = 1$, $M_2 = 1/2$, $a = 3/4$, $\lambda_2 = 3$. If making Taylor expansion for Eq. (19) at $\lambda = \lambda_1$, and without Taylor expansion at $\lambda = \lambda_2$, from Eq. (8) we can obtain the mixed hyperbolic-rational solutions as

$$\begin{aligned}\widetilde{X}_n &= a_{n+1}^{(0)} X_n + b_{n+1}^{(0)} Y_n - c_{n+1}^{(3)},\\ \widetilde{Y}_n &= a_{n+1}^{(0)} Y_n - b_{n+1}^{(0)} X_n - d_{n+1}^{(3)},\end{aligned} \tag{23}$$

where $a_{n+1}^{(0)}$, $b_{n+1}^{(0)}$, $c_{n+1}^{(3)}$ and $d_{n+1}^{(3)}$ can be given by replacing n in $a_n^{(0)}$, $b_n^{(0)}$, $c_n^{(3)}$ and $d_n^{(3)}$ with $n+1$, in which $a_n^{(0)} = \frac{\Delta a_n^{(0)}}{\Delta_2^{\varepsilon(2)}}$, $b_n^{(0)} = \frac{\Delta b_n^{(0)}}{\Delta_2^{\varepsilon(2)}}$, $c_n^{(3)} = \frac{\Delta c_n^{(3)}}{\Delta_2^{\varepsilon(2)}}$ and $d_n^{(3)} = \frac{\Delta d_n^{(3)}}{\Delta_2^{\varepsilon(2)}}$ with

$$\Delta_2^{\varepsilon(2)} = \begin{vmatrix}
\lambda_1^2\Psi_{1,n}^{(0)}(\lambda_1) & \Psi_{1,n}^{(0)}(\lambda_1) & \lambda_1^2\Psi_{2,n}^{(0)}(\lambda_1) & \Psi_{2,n}^{(0)}(\lambda_1) & -\lambda_1\Psi_{3,n}^{(0)}(\lambda_1) & -\lambda_1^3\Psi_{3,n}^{(0)}(\lambda_1) & -\lambda_1\Psi_{4,n}^{(0)}(\lambda_1) & -\lambda_1^3\Psi_{4,n}^{(0)}(\lambda_1)\\
\lambda_1^2\Psi_{2,n}^{(0)}(\lambda_1) & \Psi_{2,n}^{(0)}(\lambda_1) & -\lambda_1^2\Psi_{1,n}^{(0)}(\lambda_1) & -\Psi_{1,n}^{(0)}(\lambda_1) & \lambda_1\Psi_{4,n}^{(0)}(\lambda_1) & \lambda_1^3\Psi_{4,n}^{(0)}(\lambda_1) & -\lambda_1\Psi_{3,n}^{(0)}(\lambda_1) & -\lambda_1^3\Psi_{3,n}^{(0)}(\lambda_1)\\
\lambda_1^2\Psi_{3,n}^{(0)}(\lambda_1) & \lambda_1^4\Psi_{3,n}^{(0)}(\lambda_1) & \lambda_1^2\Psi_{4,n}^{(0)}(\lambda_1) & \lambda_1^4\Psi_{4,n}^{(0)}(\lambda_1) & \lambda_1^3\Psi_{1,n}^{(0)}(\lambda_1) & \lambda_1\Psi_{1,n}^{(0)}(\lambda_1) & \lambda_1^3\Psi_{2,n}^{(0)}(\lambda_1) & \lambda_1\Psi_{2,n}^{(0)}(\lambda_1)\\
\lambda_1^2\Psi_{4,n}^{(0)}(\lambda_1) & \lambda_1^4\Psi_{4,n}^{(0)}(\lambda_1) & -\lambda_1^2\Psi_{3,n}^{(0)}(\lambda_1) & -\lambda_1^4\Psi_{3,n}^{(0)}(\lambda_1) & -\lambda_1^3\Psi_{2,n}^{(0)}(\lambda_1) & -\lambda_1\Psi_{2,n}^{(0)}(\lambda_1) & \lambda_1^3\Psi_{1,n}^{(0)}(\lambda_1) & \lambda_1\Psi_{1,n}^{(0)}(\lambda_1)\\
\lambda_2^2\Psi_{1,n}(\lambda_2) & \Psi_{2,n}(\lambda_2) & \lambda_2^2\Psi_{2,n}(\lambda_2) & \Psi_{2,n}(\lambda_2) & -\lambda_2\Psi_{3,n}(\lambda_2) & -\lambda_2^3\Psi_{3,n}(\lambda_2) & -\lambda_2\Psi_{4,n}(\lambda_2) & -\lambda_2^3\Psi_{4,n}(\lambda_2)\\
\lambda_2^2\Psi_{2,n}(\lambda_2) & \Psi_{2,n}(\lambda_2) & -\lambda_2^2\Psi_{1,n}(\lambda_2) & -\Psi_{1,n}(\lambda_2) & \lambda_2\Psi_{4,n}(\lambda_2) & \lambda_2^3\Psi_{4,n}(\lambda_2) & -\lambda_2\Psi_{3,n}(\lambda_2) & -\lambda_2^3\Psi_{3,n}(\lambda_2)\\
\lambda_2^2\Psi_{3,n}(\lambda_2) & \lambda_2^4\Psi_{3,n}(\lambda_2) & \lambda_2^2\Psi_{4,n}(\lambda_2) & \lambda_2^4\Psi_{4,n}(\lambda_2) & \lambda_2^3\Psi_{1,n}(\lambda_2) & \lambda_2\Psi_{1,n}(\lambda_2) & \lambda_2^3\Psi_{2,n}(\lambda_2) & \lambda_2\Psi_{2,n}(\lambda_2)\\
\lambda_2^2\Psi_{4,n}(\lambda_2) & \lambda_2^4\Psi_{4,n}(\lambda_2) & -\lambda_2^2\Psi_{3,n}(\lambda_2) & -\lambda_2^4\Psi_{3,n}(\lambda_2) & -\lambda_2^3\Psi_{2,n}(\lambda_2) & -\lambda_2\Psi_{2,n}(\lambda_2) & \lambda_2^3\Psi_{1,n}(\lambda_2) & \lambda_2\Psi_{1,n}(\lambda_2)
\end{vmatrix},$$

and $\Delta a_n^{(0)}$, $\Delta b_n^{(0)}$, $\Delta c_n^{(3)}$ and $\Delta d_n^{(3)}$ are obtained by replacing the second, fourth, sixth and eighth column of $\Delta_2^{\varepsilon(2)}$ with

$$(-\lambda_1^4\Psi_{1,n}^{(0)}(\lambda_1), -\lambda_1^4\Psi_{2,n}^{(0)}(\lambda_1), -\Psi_{3,n}^{(0)}(\lambda_1), -\Psi_{4,n}^{(0)}(\lambda_1),\ -\lambda_2^4\Psi_{1,n}(\lambda_2), -\lambda_2^4\Psi_{2,n}(\lambda_2), -\Psi_{3,n}(\lambda_2), -\Psi_{4,n}(\lambda_2))^{\mathrm{T}}$$

respectively. The structures of solutions (23) are shown in Fig. 14.

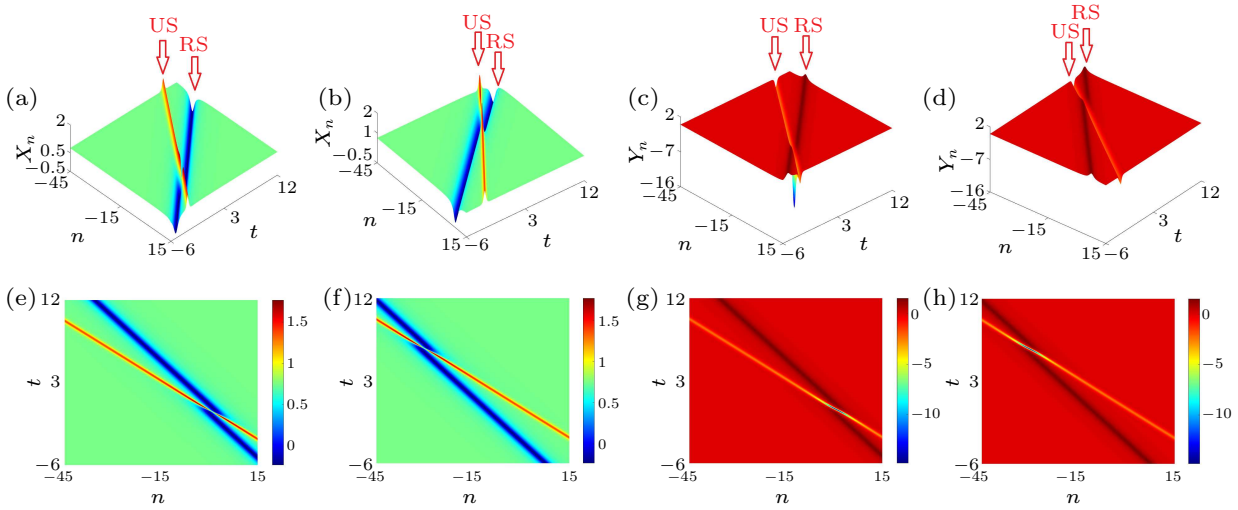


Fig. 14. Mixed interaction solutions of US and RS: [(a), (c), (e), (g)] $e_0 = 0$; [(b), (d), (f), (h)] $e_0 = 2$.

Under the effect of e_0, the position of the first-order RS has shifted, while the US keeps the position unchanged, that is to say, the parameter e_0 can change the interaction position of the US and RS, so we can control the occurrence of the interaction position by changing the parameter.

In theory, the discrete generalized $(r, N-r)$-fold DT can be extended to give more higher-order mixed interaction solutions among US, SRS and RS, but due to the complexity of actual calculations, further study is needed.

4. Conclusions

The discrete coupled mKdV equation (2) with fourth-order Lax pair has been considered systematically, which may describe the motion of shallow water waves, the optical soliton propagation in cubic nonlinear media and the Alfven wave in a cold collision-free plasma. The main innovative results of the present study are as follows:

(i) Equation (2) has been mapped to the continuous coupled KdV equation and a new nonlinear equation without dispersion term under the continuous limits.

(ii) The discrete generalized $(r, N-r)$-fold DT of Eq. (2) has been first established, from which diverse exact solutions including the usual multi-soliton, higher-order SRS, higher-order RS and their mixed hyperbolic-rational interaction soliton solutions have been given explicitly.

(iii) The asymptotic behaviors and related physical quantities of some US and RS solutions have been studied in details.

(iv) The dynamical behaviors of some exact soliton solutions are investigated via numerical simulations.

We hope the results given in this paper can provide assistance in understanding more physical phenomena in the field of shallow water wave, optics and plasma.

Acknowledgments

We would like to express our sincere thanks to other members of our discussion group for their valuable comments.

Project supported by the National Natural Science Foundation of China (Grant No. 12071042) and Beijing Natural Science Foundation (Grant No. 1202006).

References

[1] Wadati M 1976 *Prog. Theor. Phys. Suppl.* **59** 36
[2] Song Y, Shi X, Wu C, Tang D and Zhang H 2019 *Appl. Phys. Rev.* **6** 021313
[3] Harvey P, Durniak C, Samsonov D and Morfill G 2010 *Phys. Rev. E* **81** 057401
[4] Gibbon J D and Eilbeck J C 1972 *J. Phys. A: Gen. Phys.* **5** L122
[5] Faddeev L D and Korepin V E 1978 *Phys. Rep.* **42** 1
[6] Ablowitz M J, Prinari B and Trubatch A D 2004 *Discrete and Continuous Nonlinear Schrödinger Systems* (New York: Cambridge University Press)
[7] Ablowitz M J 1977 *SIAM. Rev.* **19** 663
[8] Toda M 1989 *Theory of Nonlinear Lattices* (Berlin: Springer)
[9] Hirota R 1973 *J. Phys. Soc. Jpn.* **35** 286
[10] Suris Y B 2003 *The Problem of Integrable Discretization: Hamiltonian Approach* (Basel: Birkhä Verlag)
[11] Yuan C L and Wen X Y 2021 *Chin. Phys. B* **30** 030201
[12] Ablowitz M J and Ladik J F 1977 *Stud. Appl. Math.* **57** 1
[13] Tsuchida T, Ujino H and Wadati M 1998 *J. Math. Phys.* **39** 4785
[14] Zhu Z N, Zhao H Q and Wu X N 2011 *J. Math. Phys.* **52** 043508
[15] Sahadevan R and Balakrishnan S 2009 *J. Phys. A: Math. Theor.* **42** 415208
[16] Wen X Y and Hu X Y 2014 *Adv. Differ. Equ.* **213** 1
[17] Leblond H and Mihalache D 2011 *Rom. Rep. Phys.* **63** 1254
[18] Ankiewicz A and Akhmediev N 2018 *Nonlinear Dyn.* **91** 1931
[19] Kakutani T and Ono H 1969 *J. Phys. Soc. Jpn.* **26** 1305
[20] Ablowitz M J, Luo X D and Musslimani Z H 2020 *Nonlinearity* **33** 3653
[21] Prinari B 2016 *J. Math. Phys.* **57** 083510
[22] Chen M, Fan E and He J 2023 *Chaos Soliton. Fract.* **168** 113209
[23] Chen M and Fan E 2022 *Stud. Appl. Math.* **148** 1180
[24] Geng X G, Dai H H and Cao C W 2003 *J. Math. Phys.* **44** 4573
[25] Wen X Y 2011 *Rep. Math. Phys.* **68** 211
[26] Xu T, Chen Y and Lin J 2017 *Chin. Phys. B* **26** 120201
[27] Wen X Y, Yan Z and Malomed B A 2016 *Chaos* **26** 123110
[28] Wen X Y, Liu Y and Yan Z 2015 *Phys. Rev. E* **92** 012917
[29] Cui X Q, Zhang B J and Wen X Y 2023 *Chin. J. Phys.* **82** 95
[30] Wen X Y 2016 *Commun. Theor. Phys.* **66** 29
[31] Wen X Y and Wang H T 2021 *Appl. Math. Lett.* **111** 106683
[32] Wang H T and Wen X Y 2019 *Pramana-J. Phys.* **92** 1
[33] Liu N, Wen X Y and Wang D S 2022 *Math. Meth. Appl. Sci.* **45** 9396
[34] Wen X Y and Yuan C L 2022 *Appl. Math. Lett.* **123** 107591
[35] Liu P, Jia M and Lou S Y 2007 *Phys. Scr.* **76** 674
[36] Lou S Y, Tong B, Hu H and Tang X 2006 *J. Phys. A: Math. Gen.* **39** 513
[37] Wang D S 2010 *Nonlinear Anal.* **73** 270
[38] Korteweg D J and deVries G 1895 *Phil. Mag.* **39** 422
[39] Washimi H and Taniuti T 1966 *Phys. Rev. Lett.* **17** 996
[40] Trefethen L N 2000 *Spectral Methods in MATLAB* (Philadelphia: SIAM)